Article

Entrapment Efficiency (EE) and Release Mechanism of Rhodamine B Encapsulated in a Mixture of Chia Seed Mucilage and Sodium Alginate

María de Jesús Perea-Flores [1], Héctor Filiberto Aguilar-Morán [2], Georgina Calderón-Domínguez [2], Alitzel Belem García-Hernández [3], Mayra Díaz-Ramírez [3], Hugo Enrique Romero-Campos [4], Alejandro De Jesús Cortés-Sánchez [3,5] and Ma. de la Paz Salgado-Cruz [2,*]

[1] Centro de Nanociencias y Micro y Nanotecnologías, Instituto Politécnico Nacional, Av. Luis Enrique Erro s/n, Unidad Profesional Adolfo López Mateos, Zacatenco, Gustavo A. Madero, Ciudad de México 07738, Mexico
[2] Departamento de Ingeniería Bioquímica, Escuela Nacional de Ciencias Biológicas, Instituto Politécnico Nacional, Av. Wilfrido Massieu 399, Nueva Industrial Vallejo, Gustavo A. Madero, Ciudad de México 07738, Mexico
[3] Departamento de Ciencias de la Alimentación, División de Ciencias Biológicas y de la Salud, Universidad Autónoma Metropolitana-Unidad Lerma, Av. de las Garzas 10, El Panteón, Lerma de Villada 52005, Mexico
[4] División de Ciencias Básicas e Ingeniería, Universidad Autónoma Metropolitana-Unidad Azcapotzalco, Av. San Pablo Xalpa 180, San Martin Xochinahuac, Azcapotzalco, Ciudad de México 02128, Mexico
[5] Consejo Nacional de Ciencia y Tecnología (CONACyT), Av. Insurgentes Sur 1582, Crédito Constructor, Benito Juárez, Ciudad de México 03940, Mexico
* Correspondence: msalgadoc@ipn.mx

Abstract: Chia seed mucilage is a polysaccharide capable of forming hydrogels with excellent water-binding capacity due to its physical and chemical properties and favorable characteristics for encapsulating and protecting valuable hydrophilic molecules in the food, pharmaceutical, and cosmetic industries. This research aimed to show that mixtures of chia seed mucilage and sodium alginate used as wall materials to encapsulate hydrophilic molecules are suitable. We analyzed the relationship between the mucilage–alginate solution's properties and the capsules obtained; we quantified the entrapment efficiency (EE%) and the release of rhodamine B; and we proposed a method to follow the rhodamine B release using confocal laser scanning microscopy (CLSM). We found that more viscous solutions are obtained when the mucilage concentration increases, making it difficult to produce capsules with less sphericity. The best entrapment efficiency was found when the proportion of the polymers was close to 1:1, based both on the properties of the capsules obtained and on the characterization of the release kinetics of rhodamine B; the analysis performed by fitting rhodamine B release data to theoretical models describe the diffusion process. Our results show that the use of chia seed mucilage as a wall material to trap and retain hydrophilic molecules is convenient.

Keywords: chia seed mucilage; release; entrapment

1. Introduction

In recent years, the use of chia seeds has increased due to their high protein, fatty acid, and fiber content. However, one of the most important components of these seeds is their mucilage, a hetero-polysaccharide produced by the expansion and rupture of the primary wall of specialized epidermal cells found in the coating of different types of seeds [1,2]. The mucilage is released when the seeds are submerged in water, a mechanism that presumably occurs for their protection, energy reserve, dispersal, and transport of water and/or hydration; despite this, its physiological role is unclear [2–7]. Chemically, chia seed mucilage has a high concentration of hydroxyl groups, sugars (xylose and glucose), neutral sugars (arabinose and galactose), and uronic acids (glucuronic acid and galacturonic acid), which promote the water-binding capacity [8–12], viscosity, cohesive,

and adhesive properties and the formation of weak gels formed mainly by electrostatic interactions [10,13]. In addition, this presents a structure in the form of nanometric fibers [7]. Currently, these polysaccharides extracted from chia seeds have been used in the food industry as an additive (fat substitute, thickener, emulsifier, stabilizer, texture modifier, or gelling agent), fiber source, edible films, coatings, as a wall material for the fabrication of chia seed oil nanocapsules [14,15], and/or in the pharmaceutical and cosmetic industries for the manufacture of release capsules [16–18]. It is important to note that this material also presents benefits in terms of its biodegradability, biocompatibility, abundance in nature, and low cost [16,19]. In this sense, and given its physical and chemical characteristics, it can also be used as a wall material to produce capsules or films to control release, since it can be retained or absorbed by hydrophilic or low molecular weight molecules such as rhodamine B [20]. It is worth mentioning that some authors indicate that encapsulating low-molecular-weight hydrophilic drugs into polymers is a challenging task [21], so it is necessary to look for new wall materials that meet these needs and contribute to reducing bursting release [22]. Hence, mucilage is a very promising material for use as a wall material. In addition to the above, it is also necessary to evaluate the influence of the physicochemical properties (density, viscosity, and surface tension) of the solution formed by the different polymers on the formation of the capsule and its release mechanism.

Otherwise, in the last few years, many studies have been incorporating drugs or molecules of interest to the food industry in sodium alginate matrices through the coacervation technique as a technological option to preserve and provide integrity and stability [23]. Nevertheless, the release rate of this material has some disadvantages due to its lack of mechanical and chemical stability [24]. Some research indicates that the encapsulation of water-soluble substances or enzymes in alginate beads presents problems of enzymatic stability and low entrapment efficiency [25,26]. Therefore, it is necessary to evaluate combined matrices that increase the cross-linking and retention of the molecules of interest. On the other hand, the study of the release kinetics of occluded molecules within a polymeric matrix through various mathematical models allows the calculation of constants providing useful information related to the mechanism by which the release process occurs. In addition, mathematical models such as Higuchi's, Korsmeyer's, or Peppas–Sahlin's enable a better understanding of this phenomenon, and have been developed and applied to evaluate the mucilage influence on the hydration rate as well as different wall materials in the release of molecules of interest.

From another perspective, it is also important to investigate and evaluate new techniques that are fast and economical, which allows the analysis and visualization of the efficiency of the encapsulation process when using new polymers such as mucilage from chia seeds. The most-used techniques are scanning electron microscopy (SEM) and light microscopy (LM). However, these techniques require pre-treatment and do not allow visualization of internal structures [27]. Hence, techniques such as confocal laser scanning microscopy (CLSM) represent a clear advantage over conventional light microscopy, because it allows easy localization and three-dimensional visualization along the x, y, and z axes of the entrapment of molecules, as well as observation of the interaction or distribution of the wall material. Additionally, it is a non-destructive technique that offers the possibility to quantify the encapsulated phase.

Therefore, this study aimed to evaluate the effect on the entrapment efficiency (EE%) of rhodamine B in capsules of a combined matrix of chia seed mucilage and sodium alginate as wall material, as well as to understand the mechanism of release and diffusion through different kinetic models.

2. Materials and Methods

2.1. Materials

Mucilage was extracted from chia seeds (*Salvia hispanica* L.; harvested in 2009; 21.2 ± 0.2 g protein/100 g sample (db), 6.0 ± 0.08 g ash/100 g sample (db), 36.7 ± 0.6 g fat/100 g sample

(db)) provided by producers in municipality La Palma (Nopala de Villagrán, Hidalgo, Mexico) and following the methodology proposed by Salgado-Cruz [7].

Before use, the mucilage was dried at 40 °C for 4 h in an oven (TERLAB MR, Mod: MAH25D, Zapopan, Jalisco, Mexico) until reaching a humidity of 6.0% (db). Then, it was ground and sieved (KRUPS ground, Mod: GX410011, Germany), while sodium alginate was used as purchased (Sigma-Aldrich, 9005-38-3, St. Louis, MI, USA).

2.2. Chia Seed Mucilage–Alginate Solutions

Solutions of chia seed mucilage–alginate (M–A) were prepared at different ratios and up to a final concentration of 1% *w/v*, as shown in Table 1. Then, rhodamine B (Sigma Aldrich, 83689, St. Louis, MI, USA), at 2% *w/v* in water, was added to each formulation at 0.1% *w/v*.

Table 1. Mucilage–alginate solutions at 1% *w/v*, used for the encapsulation process.

Mucilage Concentration (MU% w)	Alginate Concentration (A% w)
0.7	0.3
0.5	0.5
0.3	0.7
0.0	1.0

2.3. Rheological and Physical Characterization of Solutions

Surface tension, density, and rheological parameters of the solutions were measured as follows:

1. Surface tension (γ; dyn/cm): The surface tension of solutions was determined by the Du Noüy ring method using a tensiometer (K6, Krüss, Hamburg, Germany) coupled with a platinum–iridium ring (1.9 cm). Before each measurement, the ring and container were cleaned with distilled water and kept directly into the fire to eliminate residues. The analysis was carried out at room temperature (25 °C) and per quintuple [28].
2. Density (ρ; g/cm^3): The density of the solutions was measured using a 10 mL pycnometer. For this, the pycnometer was weighed empty and with distilled water. Then, each determination was made in triplicate at 25 °C.
3. Rheology: Rheological measurements of the mucilage–alginate solutions were performed using a Compact Modular Rheometer (Hybrid DH3 Discovery, TA Instruments, New Castle, DE, USA) equipped with a parallel plates system (40 mm diameter). Briefly, a continuous shear rate of 1 to 100 s^{-1} at 25 °C with a plate gap of 5921. A length of 31 µm was applied to determine rheological values. Moreover, the data were fitted to the Newtonian, Bingham, Casson, Power Law, and the Herschel–Bulkley ($\sigma = \sigma_0 + K\gamma^n$) models, the latter showing the best fitting to correlate the variations of the rheological behavior under constant shear, where σ is the shear stress (Pa), σ_0 is yield stress, γ is the shear rate (s^{-1}), K is the consistency coefficient (Pa·s), and n$_r$ is the flow behavior index (n$_r$, dimensionless; shear thinning n$_r$ < 1 or shear thickening n > 1) [29]. All the determinations were performed in triplicate to guarantee reproducibility. Finally, the best model was selected based on the maximum determination coefficient (R^2) and the minimum root means square error (RMSE).

2.4. Rhodamine B Encapsulation in Chia Mucilage and Alginate

The capsules were prepared following the methodology proposed by Ghumman et al., 2022 [30], with some modifications. In brief, each formulation was prepared with a mixture of dried chia seed mucilage, sodium alginate, and water (1% *w/v*) (Table 1); then, a solution of Rhodamine B was added, vortexed gently, and placed in a 0.3 mL insulin syringe (BD ultra-fine 30G, nominal inner diameter 0.159 mm, capillary length 13 mm, Becton, Dickinson

and Company, Franklin Lakes, NJ, USA). Later, the solution (0.3 mL) was added dropwise into 30 mL of a 2% *w/v* $CaCl_2$ solution. The obtained capsules were preserved in a clear $CaCl_2$ solution. Finally, for further analysis, they were separated with a sieve.

2.5. Capsules Image Analysis

Capsules' size (area) and shape (circularity, major and minor axes) were measured using the free ImageJ software, version 1.41 (ImageJ, Rasband, WS, Bethesda, MD, USA, National Institutes of Health, Bethesda, MD, USA). For this purpose, optical images (2048 × 1536 pixels) [7] taken with a stereoscopic microscope (2.5×, Nikon SMZ 1500, Tokyo, Japan,) equipped with a digital camera (Nikon DS-2Mv, Tokyo, Japan) and a fluorescent ring light, adjusted to medium intensity (Universal driver model 13 plus, USA) to ensure the homogeneity of the light and reduce the shadows of images, was used. Images were acquired using NIS-Elements F 2.30 software (Nikon, Tokyo, Japan) in sRGB color, saved in TIFF format, and converted to grayscale (8-bit). The image analysis procedure was performed as follows: the capsule contour was selected using the "wand (tracing)" command. Then, the noise was removed using the "clear outside" tool. After that, the image was filled with the "fill" tool, and finally, the required parameters were defined. This analysis was performed in triplicate.

2.6. In Vitro Release Kinetics of Rhodamine B

Rhodamine B kinetics were carried out in a UV–vis spectrophotometer (Genesys 10uv Thermo Scientific, Waltham, MA, USA) at 580 nm. Initially, 10 g of the capsules were placed in a $CaCl_2$ solution. Subsequently, an aliquot of this solution (1 mL) was read in the spectrophotometer every 30 min, from 0 to 180 min.

The release kinetics of Rhodamine B were carried out in a spectrophotometer (Thermo Scientific Genesys 10UV, Waltham, MA, USA) at 580 nm by using the solution where capsules with Rhodamine B were stored. Initially, 10 g of the capsules were put in a $CaCl_2$ solution. Subsequently, an aliquot of this solution (1 mL) was placed in the spectrophotometer bucket to perform measurements at regular intervals of time: 0, 30, 60, 90, 120, 150, 180 min. Then, to ensure the level of confidence of the UV–vis absorbance, a standard curve ($R^2 = 0.99$) was constructed based on the dye (range 0–2 mg/mL) in a $CaCl_2$ solution. Finally, the entrapment efficiency (EE%) of rhodamine B in the capsules was calculated according to Equation 1. The data obtained in the spectrophotometer were analyzed using Sigma Plot 12.0 software (Systat Software Inc., San Jose, CA, USA).

$$EE\% = \frac{\text{mg Rod Bc} - \text{mg Rod Bt}}{\text{mg Rod BC}} \times 100 \tag{1}$$

where mg Rod Bc is the initial theoretical concentration of rhodamine B in the capsules, mg Rd Bt is the concentration of rhodamine B that spreads into the $CaCl_2$ solution at different times.

2.7. Kinetic Models of Rhodamine B Release

The kinetics values of entrapment efficiency (EE%) obtained previously were fitted to the models of (1) Korsmeyer and Peppas, (2) Ritger and Peppas, and (3) Peppas and Sahlin to evaluate the behavior of rhodamine B in the matrix capsules with chia seed mucilage, as proposed by Salgado-Cruz et al., 2013 [7]. These models explain the release mechanism of the molecules encapsulated in polymeric matrices.

The first model is the Korsmeyer and Peppas, Equation (2), which describe the phenomena based on a "power law", predicting the diffusion of water into the matrix, matrix swelling, and matrix dissolution as simultaneous mechanisms [31].

$$\left(\frac{M_t}{M_\infty}\right) = k_{KP} t^n \tag{2}$$

where M_t is the amount of the rhodamine B released over time (t), M_α is the maximum amount of rhodamine B in the solution, and $k_{KP}(s^{-n})$ is a constant incorporating structural and geometric characteristics of the release system and "n" is a diffusional exponent which depends on the release mechanism.

The second model is Ritger and Peppas, Equation (3), which is a semiempirical expression that studies the release kinetics of active ingredients from flat systems in which Fickian diffusion and a combination of non-Fickian and anomalous transport also occur, called II, which describes the release mechanism of a concentration-dependent system.

$$\left(\frac{M_t}{M_\alpha}\right) = k_1 \sqrt{t} + k_2 t \tag{3}$$

where $k_1(s^{-0.5})$ represents the contribution of Fickian mechanism while $k_2(s^{-1})$ is the relaxation mechanism of the polymer chains [32].

The third model, Peppas and Sahlin, Equation (4), describes the drug release from an insoluble matrix that is directly proportional to the square root of time and is based on Fickian diffusion.

$$M_t = k_{PS1}t^n + k_{PS2}t^{2n} \tag{4}$$

where $k_{PS1}(s^{-n})$ and $k_{PS2}(s^{-2n})$ are the kinetics constants associated with the release by diffusion and relaxation, respectively, and "n" is the diffusional exponent indicative of the release mechanism for a system with any shape.

2.8. Evaluation of Rhodamine B Entrapment Efficiency into the Capsules Using Confocal Laser Scanning Microscopy (CLSM)

Briefly, 4–5 samples were taken and rinsed with 2 mL of water (four times). Subsequently, a drop of water was coated on the capsule and placed on a glass slide. Then, the sample was analyzed with a 568 nm wavelength excitation laser for rhodamine B. The maximum emission was at 625 nm. Sample images were obtained with the CLSM (LSM 710, Carl Zeiss, Oberkochen, Baden-Wurttemberg, Germany). RGB images obtained from the z-stack were converted and analyzed to dimensional chromatic coordinates of CIELAB space (L, a *, and b *) using the ImageJ software (National Institutes of Health, Bethesda, MD, USA). This was performed by obtaining stacked images of L *, a *, and b * with the Lab Stack tool in the Image/Type menu. Then, "Histogram" was selected from the Analyze menu. Finally, the mean values of the CIELAB: a * and L (luminosity) parameters were quantified for each image.

2.9. Capsules Surface Morphology by Scanning Electron Microscopy

The evaluation of the morphology and structure of the capsules was carried out by Scanning Electron Microscopy (SEM; JSM-7800F, JEOL, Tokyo, Japan) coupled with a microanalysis detector for energy-dispersive X-ray Spectroscopy (EDAX, APOLLO-XL, Mahwah, NJ, USA). The capsules were lyophilized for 4 h at −50 °C (Labconco 75,034 Bench Top Freeze Dryer from Labconco, Kansas City, MO, USA). Each specimen was mounted on conductive metal slides on double-sided carbon tape and then sputter-coated with gold using an SPI Sputter Coater module (SPI Supplies, West Chester, PA, USA). The accelerating voltage for the SEM studies was 5 kV.

2.10. Statistical Analysis

Sigma Plot V. 12.0 (Systat Software Inc., San Jose, CA, USA) and Wolfram Mathematica V. 13.1 (Wolfram, IL, USA) were used for analysis of unidirectional variance (ANOVA) and model release evaluation, respectively. At least three independent samples were carried out for each experiment. Results are shown as mean ± standard deviation.

3. Results

3.1. Rheological and Physical Characterization of Solutions

The rheological behavior of different solutions changes according to the mucilage–alginate concentration, as shown in Figure 1. Here, it is essential to highlight that greater shear thinning is detected [33,34] when the mucilage concentration is higher than the alginate concentration, as shown in the graph of Figure 1A, with a steeper slope when the viscosity of the solution decreases with increasing shear velocity. The highest viscosity was for chia seed mucilage, as reported by Naveed et al. [35,36], when comparing against barley root and maize root mucilage, but at a single concentration. This pseudoplastic characteristic can be attributed to the expansion of polysaccharide chains when they begin to hydrate, as reported by Simas-Tosin et al. [37], who suggest electrostatic intermolecular repulsion in peach gum exudates induces the formation of more viscous solutions; this also occurs with chia mucilage as observed in Figure 1A. Flow curves also demonstrate that this property is shear stress dependent. In this regard, the behavior of the dynamic flow (shear stress vs. shear velocity) of the solutions at different concentrations of mucilage and alginate is depicted in Figure 1B. Here, it is observed that at low shear rates (0.001 s^{-1}), the shear stress increases with the mucilage concentration (Figure 1B) and then decreases slightly as shear rates improve, observing a linear trend when the alginate concentration increases (Figure 1B). These results were fitted to the Herschel–Bulkley model: $\sigma = \sigma_0 + K\gamma^n$ to relate the variations in rheological behavior under constant shear, where n is the flow behavior index, and two types of phenomena, shear thinning ($n < 1$) or shear thickening ($n > 1$) [29], typical behaviors of pseudoplastic macromolecular systems, occur for both polymers [38–40].
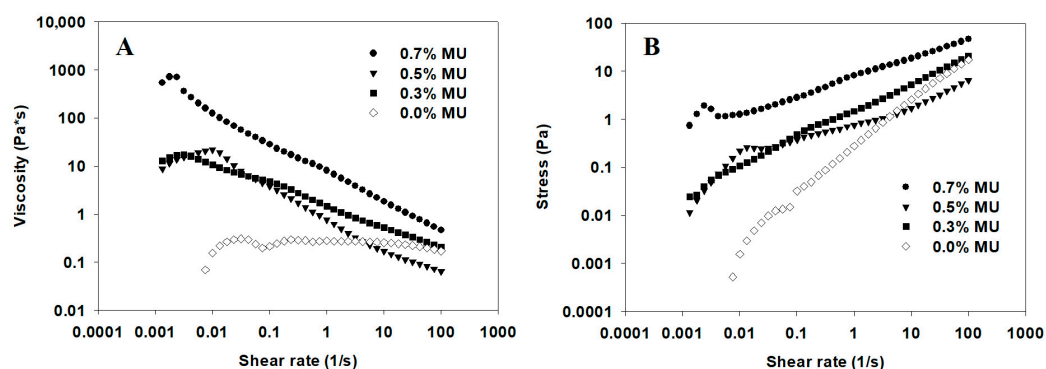

Figure 1. Rheological properties: (**A**) shear rate vs. viscosity and (**B**) stress vs. shear rate at different concentrations of mucilage–alginate.

These results may also be related to the mucilage composition, since some studies report that although the mucilage has a similar uronic acid content to low-methoxy pectin, the interactions that occur are different. Mucilage is mainly governed by weak electrostatic interactions between entangled polymer chains [11,13], which is why shear thinning could be explained by how the mucilage hydrates, which can form small aggregates in a similar way to that reported by Li et al. [41] for Arabic gum.

Changes in intrinsic viscosity could also be used to track the macromolecular interactions and capacity of entrapment or release during the encapsulation process, given the hydration capacity of the chia seed mucilage and the high content of hydroxyl (−OH) groups that are the major source of bioadhesion or adsorption [42]. Regarding the above, Cortés-Camargo et al. [43] emphasize that the mesquite gum solution presenting low viscosity brings about very rapid diffusion and anchoring of gum molecules into the oil–water interface when microencapsulating lemon essential oil. On the other hand, some research shows that natural polysaccharide fibers have a high affinity for polar dyes due to hydrogen bonding and dipole interactions [44,45]. Therefore, chia seed mucilage, by

generating higher viscosities, could have a greater retention capacity of molecules such as rhodamine B.

Table 2 shows the results of flow curve data fitting using a Herschel–Bulkley rheology model. The best fit was evaluated through the coefficient of determination R^2 and the lowest value of the minimum mean square error (RMSE), showing that all the solutions follow a thinning behavior due to index values of (*n*) less than 1, which explains the non-Newtonian pseudoplastic behavior. The results showed that the addition of alginate increased the flow behavior index, indicating a decrease in pseudo-elasticity.

Table 2. Rheological and physicochemical parameters of the solutions at different mucilage–alginate concentrations.

Mucilage Concentration (%)	Herschel–Bulkley Model				Density (g/cm^3)	Surface Tension (dyn/cm)
	R^2	RMSE	n_r (Dimensionless)	K(Pa·s^n)		
0.7	0.9985	0.3997	0.386 ± 0.0 [a]	7.57 ± 0.29 [a]	0.75 ± 0.006 [a]	80.33 ± 0.58 [a]
0.5	0.9948	0.1081	0.599 ± 00 [b]	0.39 ± 0.01 [b]	0.82 ± 0.0 [b]	62.67 ± 0.06 [b]
0.3	0.9998	0.0896	0.595 ± 0.01 [c]	1.328 ± 0.05 [c]	0.93 ± 0.0 [c]	62.67 ± 0.58 [b]
0	0.9997	0.1099	0.801 ± 0.00 [d]	0.44 ± 0.01 [d]	0.95 ± 0.0 [d]	58.17 ± 0.58 [c]

Values are presented as mean ± standard deviation. Different lowercase letters in the same column are significantly different ($p \leq 0.05$).

Concerning the k values, they represent proportionality and are a constant parameter that shows the degree of changes in shear stress because of changes in shear rate [42]. Table 2 shows that the highest value is 7.57 Pa·s^n when the mucilage concentration is higher, which indicates that the variation of the applied cutting speed results in a more significant change in the cutting effort. These results agree with those reported by Cuomo et al. [46], where k values increased with mucilage concentration and *n* values decreased. Eventually, the non-Newtonian behavior of mucilage solutions is also critical in capsule making, which is a fundamental factor during the injection phase and can become too complex [47]. In our experiments, especially in capsules prepared at concentrations higher than 0.7% mucilage, the viscosity increased significantly, obstructing the injection and generating larger and completely deformed capsules.

Regarding the surface tension of the solutions used for the capsule production, the values showed that this physicochemical property decreased at lower mucilage concentrations. This trend has also been observed for gum solutions, such as xanthan, carrageenan [48], fenugreek [49], and basil seed gum [50]. Nevertheless, the increment in surface tension when increasing the concentration of mucilage can be attributed to the high viscosity of the solutions, as well as to the measurement technique, due to how only a part of the liquid that separates from the surface is lifted by the ring and adheres to it [51], with an error of 30% or more [52,53]. The density values increased when the mucilage concentration was reduced (Table 2). This occurred due to the hydration of the mucilage, which generated significant changes in its volume [7,54].

3.2. Capsules Image Analysis

The stereoscopic microscope images (Figure 2) of the capsules obtained showed that the hemispherical shapes increase depending on the mucilage concentration. This effect could be attributed to an increase in the viscosity and surface tension of the mix, since they affect the injection flow, which generates pear-shaped or teardrop-shaped matrix capsules (Figure 2), as reported by Davarcı et al. [55]. As for the alginate, smooth surfaces and spherical shapes are observed when the concentration increased (Figure 2, 0% Mu), which has also been reported by Macías-Cortés et al. [23] and Rentería-Ortega et al. [56], who found that the dripping mode generates less capsule deformation than those produced by electrohydrodynamic (EHD) atomization when chia seed mucilage is used for glucose oxidase encapsulation.
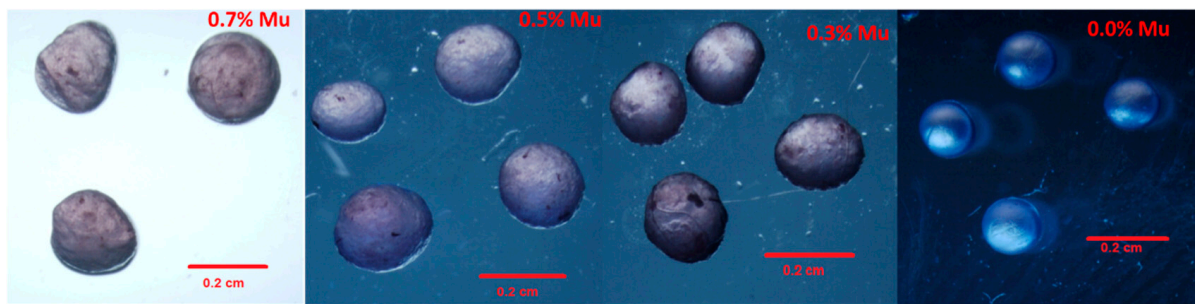
Figure 2. Shapes of the capsules obtained for the solutions at different mucilage and alginate concentrations.

The determination of the shape of the capsules (diameter, major and minor axes, and circularity) is shown in Table 3. Here, the average diameter varies from 0.15 to 0.24 cm; the lowest values correspond to the samples with the highest alginate content, and the largest particle size was obtained when a high concentration of mucilage was used (0.7% Mu). On the other hand, the major and minor axes and the measures of circularity were significantly different between the samples. Likewise, the size and dimension of the droplet depend on the flow's rheology, since as the viscosity of the solutions increases, it is necessary to apply more force to extrude the droplets, producing larger capsules. These results are equivalent to those reported by Santhanes et al. [57]. It was also observed that the mean circularity values of the capsules improved when the alginate content increased (0% Mu). However, the hemispherical shape and smaller size of the capsule could have a major effect on the release of rhodamine B.

Table 3. Shape factors for each sample with different content of mucilage and alginate.

Mucilage Concentration (%)	Diameter (cm)	Major Axis (cm)	Minor Axis (cm)	Circularity
0.7	0.24 ± 0.015 [a]	0.25 ± 0.010 [a]	0.20 ± 0.008 [a]	0.84 ± 0.028 [a]
0.5	0.21 ± 0.012 [b]	0.20 ± 0.015 [b]	0.19 ± 0.010 [a]	0.85 ± 0.007 [a]
0.3	0.20 ± 0.006 [b]	0.19 ± 0.008 [b]	0.17 ± 0.007 [b]	0.86 ± 0.020 [a]
0.0	0.15 ± 0.000 [c]	0.15 ± 0.001 [c]	0.14 ± 0.002 [c]	0.89 ± 0.015 [b]

Values are presented as mean ± standard deviation. Different lowercase letters in the same column are significantly different ($p \leq 0.05$).

3.3. In Vitro Release Kinetics of Rhodamine B

Figure 3A shows the kinetics of the entrapment efficiency (EE) over 3 h. As observed, the initial EE of rhodamine B is between 94% and 96% and depends on the mucilage concentration. Indeed, the initial and final EE% at 0.5% concentration is higher than the other concentrations. However, the release of rhodamine B, measured as the difference between final and initial EE or as the slope of the EE as a function of time, did not show a simple relationship with mucilage concentration. After 3 h, the EE at concentrations of mucilage other than 0.5% is significantly lower (around 93% vs. higher than 94%). When mucilage concentrations are greater than 0.5%, its swelling and hydration could allow rhodamine B to be more accessible, while when alginate concentrations are higher, the development of the egg-box structure could allow rhodamine B to diffuse easily. These suggest an optimal mucilage–alginate ratio, around 1:1, that improves EE.
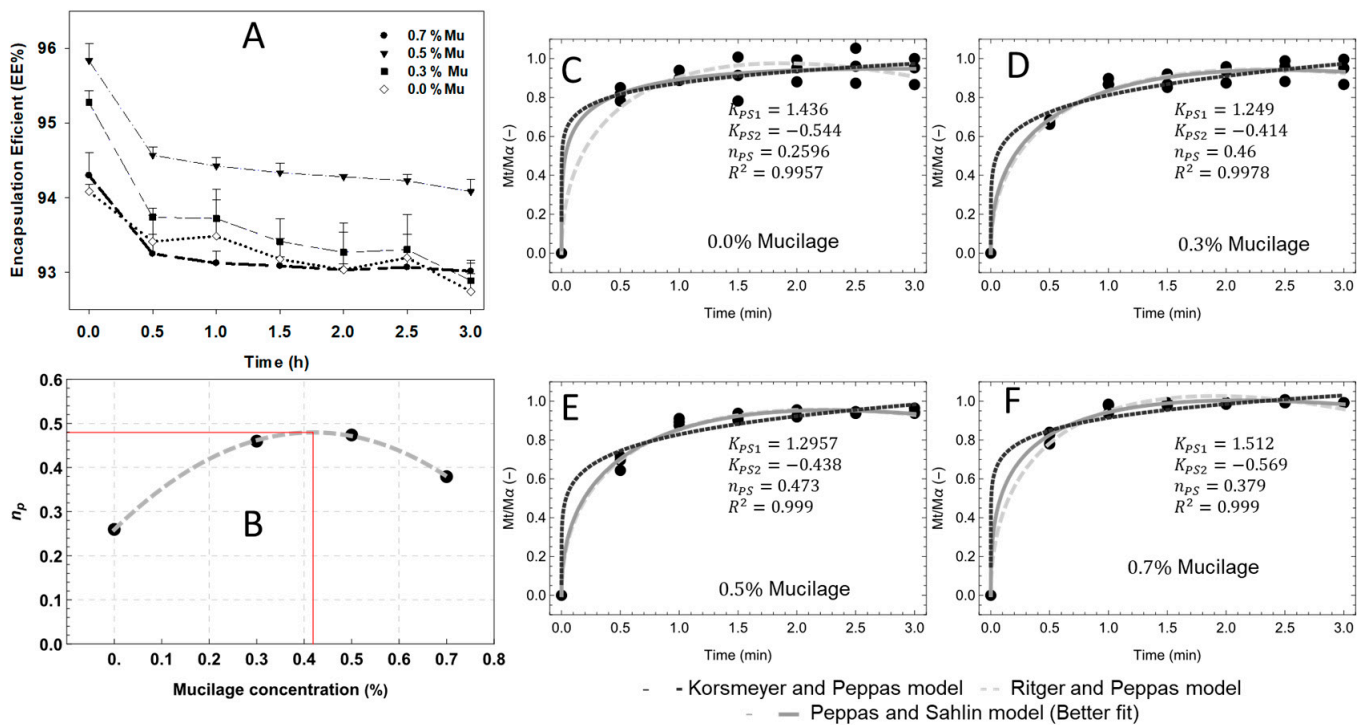
Figure 3. (**A**) Kinetic of entrapment efficiency (EE%) of rhodamine B at different mucilage concentrations; (**B**) optimal mucilage concentration in function of exponent "*n*"; (**C–F**) release profile of rhodamine B fitted to the Peppas and Sahlin model. M_t and M_α represent the amount of rhodamine B released at time "t" and at infinite time "α", respectively.

Even so, viscosity of the solution does not allow easy production of capsules, as observed in the loss of sphericity. Figure 3B shows that after the encapsulation process, the rhodamine B release in water was fast during the first hour and showed sustained release for the rest of the time. This could occur because the rhodamine B molecule forms a matrix with the polymers and is adsorbed on the surface, producing an unavoidable lixiviation of the molecules, as reported by Estrada-Villegas et al. [58], indicating that the "burst" effect occurs during the first stage, due to superficial desorption. However, rhodamine B release is lower when a higher concentration of chia seed mucilage is used, a behavior related to the solution's viscosity and the high water-binding capacity, which may block the pores on the surface; results consistent with the results reported by Nayak et al. [59]. However, the rhodamine B release profile also depends on different parameters such as shape, size, and type of the capsule, ionic strength, and physicochemical properties of the mucilage–alginate matrix. Another explanation may be the high adsorption capacity due to the existence of nanometric fibers [7] and intrinsic microporous structure [60], which may facilitate the entrapment of small molecules. However, it is necessary to determine whether the adsorption process is governed only by intraparticle diffusion or if it is more complex and involves more than only one diffusive resistance such as surface adsorption, ion exchange, complexation, complexation–chelation, or micro-precipitation, and to analyze these phenomena with other methodologies such as those reported by Javanbakht and Shafiei [61].

The capsule release profiles were fitted to three mathematical models to understand the rhodamine B release mechanism. The best fit was obtained with the Peppas and Sahlin model Figure 3C–F), showing good correlation coefficients ($R^2 = 0.995$ to 0.999). The values of *n* and K for the solutions with different concentrations of mucilage provide information on the mechanism of rhodamine B transport, proposing from these values that the dominant phenomenon is pseudo-Fickian, also known as quasi-Fickian or less-Fickian diffusion, as reported by [62–66]. Thus, *n* values of 0.2596–0.473 indicate that the water penetration rate

is less than the polymer chain relaxation rate, which slows down the release of rhodamine B molecules into water, as shown in Figure 3, which is determined by partial diffusion. Rhodamine B molecules will diffuse from a high concentration (capsule surface) to a low concentration due to the diffusion effect (immersion liquid). The molecules inside will be restricted due to the cross-linking between the mucilage and the alginate, causing less diffusion, which is convenient for hydrophilic molecules that are unstable and have low retention during encapsulation processes.

We found a quadratic correlation between the parameter "*n*" and the mucilage concentration ($R^2 = 0.999$), of which the maximum occurs when the concentration is 0.42% (Figure 3B). This finding is based on theoretical diffusion models and is consistent with the suggested existence of an optimal proportion (close to 1:1) for mucilage–alginate.

These values could also suggest that this is due to the so-called "release controlled by swelling" [67] or by degradation and swelling of the polymeric matrix (mucilage–alginate). Nevertheless, the results of this study did not show the swelling rate of the capsules concerning time, which can affect the release and entrapment, so it is necessary to carry out studies that demonstrate this phenomenon. Another primary reason is the hydration of the mucilage since it is a material with a great water-binding capacity, which could generate "less diffusion", limiting the migration of trapped molecules and determining the leaching of rhodamine B.

3.4. Evaluation of Rhodamine B Entrapment Efficiency into the Capsules Using Confocal Laser Scanning Microscopy (CLSM)

Figure 4 shows the images of the distribution of the dye in the capsules, obtained with confocal laser scanning microscopy (CLSM), studied to provide more evidence of the retention capacity of hydrophilic molecules (rhodamine B) in the matrix of alginate–mucilage. These allow observing the distribution and entrapment of rhodamine B (red areas) into the matrix of mucilage–alginate at different concentrations. These results show that at the highest mucilage concentrations, the relative signals change among the images, which is visually evident in the intensity and size of the retained particles (LRP: large retained particles). It can be qualitatively observed that the sample with the highest saturation corresponds to 0.5% mucilage −0.5% alginate, which also presents the largest retained particles (LRP); subsequently, these images were used to quantify how the perceived luminosity varies.

Table 4 shows the quantified results of rhodamine B concentration, in terms of luminosity and a*, determined from the micrographs obtained by CLSM. These results indicate that the highest values for both color space coordinates (L = 12.11 ± 1.51; a * = 22.54 ± 3.06) were found using the 0.5% mucilage and 0.5% alginate (ratio 1:1) solutions, as it was observed in the kinetics of rhodamine B release, demonstrating high retention of the analyzed molecule, which is important in the retention of encapsulation and sustained release of hydrophilic molecules because their protection remains a challenge.

3.5. Surface Morphology of Capsules by Scanning Electron Microscopy

Figure 5 shows the morphology of the capsules prepared at different concentrations of the chia seed mucilage–sodium alginate mixtures. The structural characteristics observed by this method provide a better understanding of rhodamine B retention, as well as the interaction between polymers. In this case, the effect of cross-linking on the microstructure of the lyophilized sample was observed. The micrographs show that there are crystals (Cry) on the surface of the capsule that could be attributed to the presence of sodium chloride. This phenomenon was evident when the concentration of sodium alginate was higher (3 and 0% Mu), since during the capsule's preparation, the Na^+ ions of the alginate are replaced by Ca^{2+} ions coming from the $CaCl_2$, forming sodium chloride crystals [68].

On the other hand, the freeze-drying process damaged the capsule shape, causing the outer surface of the highest mucilage concentration to show more roughness and creases (7% Mu); in addition, at this concentration, irregular (hexagonal) structures and

characteristics of cells of chia seed mucilage cells (MuC) were found, equivalent to the chia endosperm cells [7].

Regarding alginate capsules, a more porous surface was then observed (Figure 5, 0% Mu). These microstructural characteristics might be correlated with swelling and molecule release studies, because rhodamine B release was highest in capsules elaborated only with alginate, probably because micropores increase the surface area and the contact with the immersion liquid generates greater rhodamine B diffusion; these results are also corroborated by confocal microscopy.
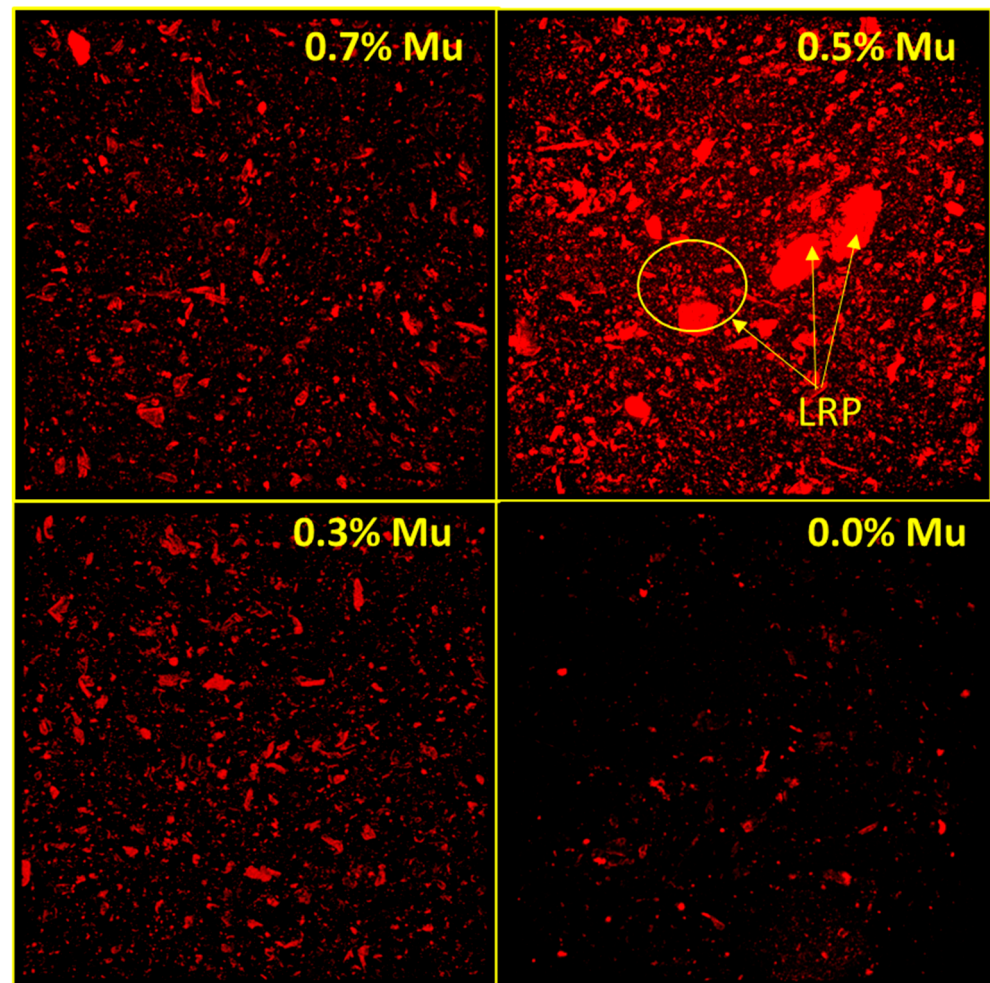

Figure 4. CSLM microphotographs of the capsules made from mucilage–alginate with rhodamine B. LRP (large, retained particles).

Table 4. L *a * color values obtained from image processing, acquired by CSLM.

Mucilage Concentration (%)	L	a *
0.7	4.99 ± 0.12 [a]	11.98 ± 0.22 [a]
0.5	12.11 ± 1.51 [c]	22.54 ± 3.06 [b]
0.3	3.94 ± 0.38 [a,d]	8.49 ± 0.81 [a,d]
0.0	1.23 ± 0.16 [e]	3.77 ± 0.52 [e]

Values are presented as mean ± standard deviation. Different lowercase letters in the same column are significantly different ($p \leq 0.05$).
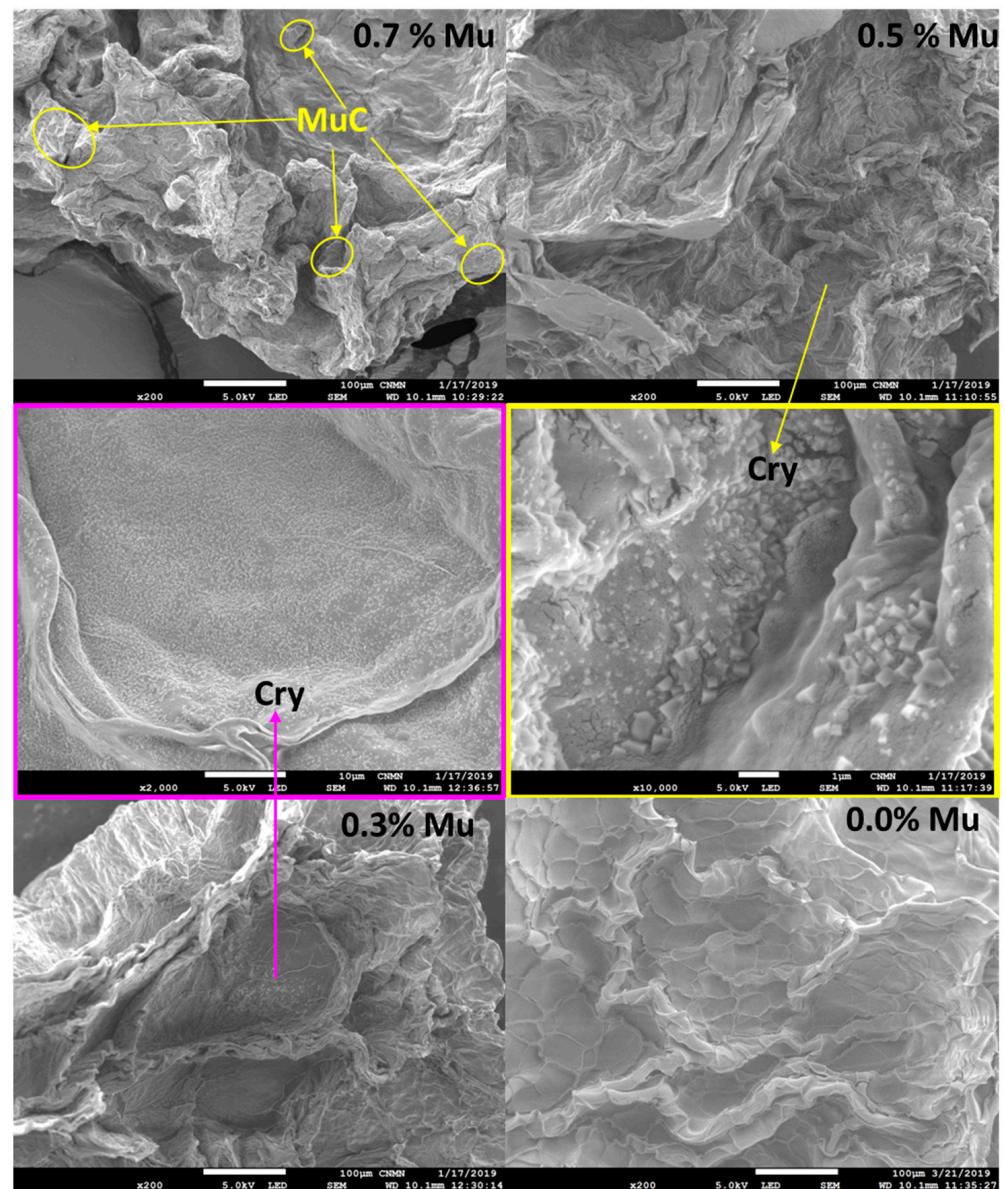
Figure 5. Microstructure of capsules matrix with mucilage–alginate. Cry (Crystal); MuC (Mucilage cells).

4. Conclusions

The initial interest of this study was to highlight the application of chia seed mucilage due to its physical (nanometric fibers) and chemical (hydroxyl groups, sugars, and uronic acids) structure since it can strengthen the structure of sodium alginate-based capsules, as well as generate higher encapsulation efficiency. In this sense, higher mucilage content was found to exhibit shear-thinning behavior, due to the nature of the polysaccharide and tweak gel-forming type. Furthermore, when the solution comes into contact with $CaCl_2$, the cross-linking process with the calcium cation is minimal, generating fewer spherical capsules but the best entrapment efficiency (EE). Therefore, due to the physicochemical and rheological properties of the chia mucilage solution, it could become an excellent functional ingredient to make capsules that retain hydrophilic molecules, where the shape is not important.

In this sense, the optimal encapsulation parameters of rhodamine B by coacervation were chia seed mucilage and sodium alginate in a 1:1 ratio, since mucilage exhibits a strong interaction and cross-linking with sodium alginate and the $CaCl_2$, forming a viscous

gel and consequently generating adequate capture efficiency ($\approx 94\%$), demonstrating the advantages of incorporating mucilage over the use of only alginate. Additionally, due to the physicochemical characteristics and the "pseudo-fickian" release mechanism present in the chia seed mucilage, our results are useful and can be applied as an excellent wall material with potential application to protect the delivery or entrapment of hydrophilic biomolecules used in the pharmaceutical and food industries. Finally, these results were also corroborated by the confocal scanning microscopy technique, which turns out to be a functional tool for the quantification and localization of encapsulated compounds.

Author Contributions: Conceptualization, M.d.J.P.-F., M.d.l.P.S.-C. and H.F.A.-M.; methodology, M.D.-R., A.D.J.C.-S. and A.B.G.-H.; software, G.C.-D. and H.E.R.-C.; validation, M.d.l.P.S.-C. and A.B.G.-H.; formal analysis, M.d.l.P.S.-C. and H.E.R.-C.; investigation, M.d.l.P.S.-C. and M.d.J.P.-F., resources, H.F.A.-M.; data curation, H.F.A.-M. and H.E.R.-C.; writing—original draft preparation, M.d.J.P.-F., M.d.l.P.S.-C. and H.F.A.-M.; writing—review and editing M.d.J.P.-F., A.B.G.-H. and M.d.l.P.S.-C.; visualization, M.d.J.P.-F., M.d.l.P.S.-C. and G.C.-D.; supervision, G.C.-D.; project administration, M.d.l.P.S.-C. and G.C.-D.; funding acquisition, M.d.J.P.-F., M.d.l.P.S.-C. and G.C.-D. All authors have read and agreed to the published version of the manuscript.

Funding: This study was supported by Instituto Politécnico Nacional (IPN), Mexico (SIP projects: 20221510), as well as by Cátedras CONACyT (1688, ID: 615).

Institutional Review Board Statement: Not applicable.

Informed Consent Statement: Not applicable.

Data Availability Statement: Not applicable.

Conflicts of Interest: The authors declare no conflict of interest.

References

1. Nazir, S.; Wani, I.A.; Masoodi, F.A. Extraction optimization of mucilage from Basil (*Ocimum basilicum* L.) seeds using response surface methodology. *J. Adv. Res.* **2017**, *8*, 235–244. [CrossRef] [PubMed]
2. Haughn, G.W.; Western, T.L. Arabidopsis Seed Coat Mucilage is a Specialized Cell Wall that Can be Used as a Model for Genetic Analysis of Plant Cell Wall Structure and Function. *Front. Plant Sci.* **2012**, *3*, 22645594. [CrossRef] [PubMed]
3. Arsovski, A.A.; Haughn, G.W.; Western, T.L. Seed coat mucilage cells of Arabidopsis thaliana as a model for plant cell wall research. *Plant Signal. Behav.* **2010**, *5*, 796–801. [CrossRef] [PubMed]
4. Western, T. The sticky tale of seed coat mucilages: Production, genetics, and role in seed germination and dispersal. *Seed Sci. Res.* **2012**, *22*, 1–25. [CrossRef]
5. Clifford, S.C.; Arndt, S.K.; Popp, M.; Jones, H.G. Mucilages and polysaccharides in Ziziphus species (*Rhamnaceae*): Localization, composition and physiological roles during drought-stress. *J. Exp. Bot.* **2002**, *53*, 131–138. [CrossRef]
6. Zimmermann, U.; Zhu, J.J.; Meinzer, F.C.; Goldstein, G.; Schneider, H.; Zimmermann, G.; Benkert, R.; Thürmer, F.; Melcher, P.; Webb, D.; et al. High Molecular Weight Organic Compounds in the Xylem Sap of Mangroves: Implications for Long-Distance Water Transport. *Bot. Acta* **1994**, *107*, 218–229. [CrossRef]
7. de la Paz Salgado-Cruz, M.; Calderón-Domínguez, G.; Chanona-Pérez, J.; Farrera-Rebollo, R.R.; Méndez-Méndez, J.V.; Díaz-Ramírez, M. Chia (*Salvia hispanica* L.) seed mucilage release characterization. A microstructural and image analysis study. *Ind. Crops Prod.* **2013**, *51*, 453–462. [CrossRef]
8. Ferrari-Felisberto, M.H.; Wahanik, A.L.; Gomes-Ruffi, C.R.; Pedrosa Silva Clerici, M.T.; Kil Chang, Y.; Joy Steel, C. Use of chia (*Salvia hispanica* L.) mucilage gel to reduce fat in pound cakes. *LWT-Food Sci. Technol.* **2015**, *63*, 1049–1055. [CrossRef]
9. Us-Medina, U.; Ruiz-Ruiz, J.C.; Quintana-Owen, P.; Segura-Campos, M.R. *Salvia hispanica* mucilage-alginate properties and performance as an encapsulation matrix for chia seed oil. *J. Food Process. Preserv.* **2017**, *41*, e13270. [CrossRef]
10. Timilsena, Y.P.; Adhikari, R.; Kasapis, S.; Ahikari, B. Molecular and functional characteristics of purified gum from Australian chia seeds. *Carbohydr. Polym.* **2016**, *136*, 128–136. [CrossRef]
11. Ellerbrock, R.H.; Ahmed, M.A.; Gerke, H. Spectroscopic characterization of mucilage (chia seed) and polygalacturonic acid. *J. Plant Nutr. Soil Sci.* **2019**, *182*, 888–895. [CrossRef]
12. Avila-de la Rosa, G.; Alvarez-Ramirez, J.; Vernon-Carter, E.J.; Carrillo-Navas, H.; Pérez-Alonso, C. Viscoelasticity of chia (*Salvia hispanica* L.) seed mucilage dispersion in the vicinity of an oil-water interface. *Food Hydrocoll.* **2015**, *49*, 200–207. [CrossRef]
13. Brax, M.; Schaumann, G.E.; Diehl, D. Gel formation mechanism and gel properties controlled by Ca^{2+} in chia seed mucilage and model substances. *J. Soil Sci. Plant Nutr.* **2019**, *182*, 92–103. [CrossRef]

14. de Campo, C.; Pereira-Dos Santos, P.; Hass-Costa, T.M.; Paese, K.; Stanisçuaski-Guterres, S.; de Oliveira-Rios, A.; Hickmann-Flôres, S. Nanoencapsulation of chia seed oil with chia mucilage (*Salvia hispanica* L.) as wall material: Characterization and stability evaluation. *Food Chem.* **2017**, *234*, 1–9. [CrossRef]

15. Fernandes-Santos, S.; Salas-Mellado, M.M. Addition of chia seed mucilage for reduction of fat content in bread and cakes. *Food Chem.* **2017**, *227*, 237–244. [CrossRef] [PubMed]

16. Prajapati, V.D.; Jani, G.K.; Moradiya, N.G.; Randeria, N.P. Pharmaceutical applications of various natural gums, mucilages and their modified forms. *Carbohydr. Polym.* **2013**, *92*, 1685–1699. [CrossRef] [PubMed]

17. Dick, M.; Hass-Costa, T.M.; Gomaa, A.; Subirade, M.; de Oliveira-Rios, A.; Hickmann-Flôres, S. Edible film production from chia seed mucilage: Effect of glycerol concentration on its physicochemical and mechanical properties. *Carbohydr. Polym.* **2015**, *130*, 198–205. [CrossRef]

18. Singh, K.; Kumar, A.; Langyan, N.; Ahuja, M. Evaluation of Mimosa pudica seed mucilage as sustained-release excipient. *AAPS PharmSciTech.* **2009**, *10*, 1121–1127. [CrossRef] [PubMed]

19. Fahami, A.; Fathi, M. Fabrication and characterization of novel nanofibers from cress seed mucilage for food applications. *J. Appl. Polym.* **2018**, *135*, 45811. [CrossRef]

20. Abd-El Hafeez, S.I.; Eleraky, N.E.; Hafez, E.; Abouelmagd, S.A. Design and optimization of metformin hydrophobic ion pairs for efficient encapsulation in polymeric drug carriers. *Sci. Rep.* **2022**, *12*, 5737. [CrossRef]

21. Yu, W.; Zhang, D.; Liu, X.; Wang, Y.; Tong, J.; Zhang, M.; Ma, X. Amphiphilic sodium alginate-vinyl acetate microparticles for drug delivery. *J. Oceanol. Limnol.* **2019**, *37*, 855–862. [CrossRef]

22. Arabi, M.; Ostovan, A.; Reza-Bagheri, A.; Guo, X.; Li, J.; Ma, J.; Chen, L. Hydrophilic molecularly imprinted nanospheres for the extraction of rhodamine B followed by HPLC analysis: A green approach and hazardous waste elimination. *Talanta* **2020**, *215*, 120933. [CrossRef] [PubMed]

23. Macías-Cortés, E.; Gallegos-Infante, J.A.; Rocha-Guzmán, N.E.; Moreno-Jiménezm, M.R.; Medina-Torres, L.; González-Laredo, R.F. Microencapsulation of phenolic compounds: Technologies and novel polymers. *Rev. Mex. Ing. Quim.* **2019**, *19*, 491–521. [CrossRef]

24. Simó, G.; Fernández-Fernández, E.; Vila-Crespo, J.; Ruipérez, V.; Rodíguez-Nogales, J.M. Research progress in coating techniques of alginate gel polymer for cell encapsulation. *Carbohydr. Polym.* **2017**, *170*, 1–14. [CrossRef] [PubMed]

25. Anjani, K.; Kailasapathy, K.; Phillips, M. Microencapsulation of enzymes for potential application in acceleration of cheese ripening. *Int. Dairy J.* **2007**, *17*, 79–86. [CrossRef]

26. Dashevsky, A. Protein loss by the microencapsulation of an enzyme (lactase) in alginate beads. *Int. J. Pharm.* **1998**, *161*, 1–5. [CrossRef]

27. Lamprecht, A.; Schäfer, U.F.; Lehr, C.M. Visualization and quantification of polymer distribution in microcapsules by confocal laser scanning microscopy (CLSM). *Int. J. Pharm.* **2000**, *196*, 223–226. [CrossRef]

28. Erfani, A.; Khosharay, S.; Aichele, C.P. Surface tension and interfacial compositions of binary glycerol/alcohol mixtures. *J. Chem. Thermodyn.* **2019**, *135*, 241–251. [CrossRef]

29. Ocampo-Salinas, I.O.; Jiménez-Aparicio, A.; Perea-Flores, M.J.; Tapia-Ochoategui, A.; Salgado-Cruz, M.P.; Jiménez-Martínez, C.; Téllez-Medina, D.I.; Dávila-Ortiz, G. High-pressure homogenization and maltodextrins mixtures to microencapsulate vanilla (*Vanilla planifolia*) extract through freeze-drying. *Rev. Mex. Ing. Quim.* **2017**, *16*, 131–146. [CrossRef]

30. Ghumman, S.A.; Mahmood, A.; Noreen, S.; Rana, M.; Hameed, H.; Ijaz, B.; Sara, H.; Aslam, A.; ur Rehman, M.F. Formulation and evaluation of quince seeds mucilage—Sodium alginate microspheres for sustained delivery of cefixime and its toxicological studies. *Arab. J. Chem.* **2022**, *15*, 103811. [CrossRef]

31. Permanadewi, I.; Kumoro, A.C.; Wardhani, D.H.; Aryanti, N. Modelling of controlled drug release in gastrointestinal tract simulation. *J. Phys. Conf. Ser.* **2019**, *1295*, 012063. [CrossRef]

32. Ritger, P.L.; Peppas, N.A. A simple equation for description of solute release I. fickian and non-fickian release from non-swellable devices in the form of slabs, spheres, cylinders or discs. *J. Control. Release* **1987**, *5*, 23–36. [CrossRef]

33. Brütsch, L.; Stringer, F.J.; Kuster, S.; Windhab, E.J.; Fischer, P. Chia seed mucilage—A vegan thickener: Isolation, tailoring viscoelasticity and rehydration. *Food Funct.* **2019**, *10*, 4854–4860. [CrossRef] [PubMed]

34. Tamargo, A.; Cueva, C.; Laguna, L.; Moreno-Arribas, M.V.; Muñoz, L.A. Understanding the impact of chia seed mucilage on human gut microbiota by using the dynamic gastrointestinal model simgi®. *J. Funct. Foods* **2018**, *50*, 104–111. [CrossRef]

35. Naveed, M.; Brown, L.K.; Raffan, A.C.; George, T.S.; Bengough, A.G.; Roose, T.; Sinclair, I.; Koebernick, N.; Cooper, L.; Hackett, C.A.; et al. Plant exudates may stabilize or weaken soil depending on species, origin and time: Effect of plant exudates on rhizosphere formation. *Eur. J. Soil Sci.* **2017**, *68*, 806–816. [CrossRef]

36. Naveed, M.; Ahmed, M.A.; Benard, P.; Brown, L.K.; Goerge, T.S.; Bengough, A.G.; Roose, T.; Koebernick, N.; Hallett, P.D. Surface tension, rheology and hydrophobicity of rhizodeposits and seed mucilage influence soil water retention and hysteresis. *Plant Soil* **2019**, *437*, 65–81. [CrossRef]

37. Simas-Tosin, F.F.; Barraza, R.R.; Petkowicz, C.L.O.; Silveira, J.L.M.; Sassaki, G.L.; Santos, E.M.R.; Gorin, P.A.J.; Iacomimi, M. Rheological and structural characteristics of peach tree gum exudate. *Food Hydrocoll.* **2010**, *24*, 486–493. [CrossRef]

38. Paolicelli, P.; Varani, G.; Pacelli, S.; Ogliani, E.; Nardoni, M.; Petralito, S.; Adrover, A.; Casadei, M.A. Design and characterization of a biocompatible physical hydrogel based on scleroglucan for topical drug delivery. *Carbohydr. Polym.* **2017**, *174*, 960–969. [CrossRef]

39. Wu, Y.; Guo, R.; Cao, N.; Sun, X.; Sui, Z.; Guo, Q. A systematical rheological study of polysaccharide from *Sophora alopecuroides* L. seeds. *Carbohydr. Polym.* **2017**, *180*, 63–71. [CrossRef]

40. Soto-Caballero, M.C.; Valdez-Fragoso, A.; Salinas-López, A.N.; Verardo, V.; Mujica-Paz, H. Rheological parameters of xanthan gum/pectin solutions as a function of temperature and composition. *Rev. Mex. Ing. Quim.* **2016**, *15*, 859–868. [CrossRef]

41. Li, X.; Fang, Y.; Al-Assaf, S.; Phillips, G.O.; Nishinari, K.; Zhang, H. Rheological study of gum arabic solutions: Interpretation based on molecular self-association. *Food Hydrocoll.* **2009**, *23*, 2394–2402. [CrossRef]

42. Deore, U.V.; Mahajan, H.S. Isolation and characterization of natural polysaccharide from Cassia Obtustifolia seed mucilage as film forming material for drug delivery. *Int. J. Biol. Macromol.* **2018**, *115*, 1071–1078. [CrossRef] [PubMed]

43. Cortés-Camargo, S.; Acuña-Avila, P.E.; Rodríguez-Huezo, M.E.; Román-Guerrero, A.; Varela-Guerrero, V.; Pérez-Alonso, C. Effect of chia mucilage addition on oxidation and release kinetics of lemon essential oil microencapsulated using mesquite gum —Chia mucilage mixtures. *Food Res. Int.* **2019**, *116*, 1010–1019. [CrossRef]

44. Maqsood, H.; Uroos, M.; Muazzam, R.; Naz, S.; Muhammad, N. Extraction of basil seed mucilage using ionic liquid and preparation of AuNps/mucilage nanocomposite for catalytic degradation of dye. *Int. J. Biol. Macromol.* **2020**, *164*, 1847–1857. [CrossRef] [PubMed]

45. Blackburn, R.S. Natural Polysaccharides and their interactions with dye molecules: Applications in effluent treatment. *Environ. Sci. Technol.* **2004**, *38*, 4905–4909. [CrossRef] [PubMed]

46. Cuomo, F.; Iacovino, S.; Cinelli, G.; Messia, M.C.; Marconi, E.; Lopez, F. Effect of additives on chia mucilage suspensions: A rheological approach. *Food Hydrocoll.* **2020**, *109*, 106118. [CrossRef]

47. Nowrouzi, I.; Mohammadi, A.H.; Khaksar, A.M. Characterization and likelihood application of extracted mucilage from Hollyhocks plant as a natural polymer in enhanced oil recovery process by alkali-surfactant-polymer (ASP) slug injection into sandstone oil reservoirs. *J. Mol. Liq.* **2020**, *320*, 114445. [CrossRef]

48. Huang, X.; Kakuda, Y.; Cui, W. Hydrocolloids in emulsions: Particle size distribution and interfacial activity. *Food Hydrocoll.* **2001**, *15*, 533–542. [CrossRef]

49. Brummer, Y.; Cui, W.; Wang, Q. Extraction, purification and physicochemical characterization of fenugreek gum. *Food Hydrocoll.* **2003**, *17*, 229–236. [CrossRef]

50. Naji-Tabasi, S.; Razavi, S.M.A.; Mohebbi, M.; Malaekeh-Nikouei, B. New studies on basil (*Ocimum bacilicum* L.) seed gum: Part I—Fractionation, physicochemical and surface activity characterization. *Food Hydrocoll.* **2016**, *52*, 350–358. [CrossRef]

51. Lee, B.B.; Chan, E.S.; Ravindra, P.; Khan, T.A. Surface tension of viscous biopolymer solutions measured using the du Nouy ring method and the drop weight methods. *Polym. Bull.* **2012**, *69*, 471–489. [CrossRef]

52. Sitthithaworn, W.; Khongkaw, M.; Wiranidchapong, C.; Koobkokkruad, T. Mucilage powder from *Litsea glutinosa* leaves stimulates the growth of cultured human hair follicles. *Songklanakarin J. Sci. Technol.* **2018**, *40*, 1076–1080. [CrossRef]

53. Huh, C.; Mason, S.G. A rigorous theory of ring tensiometry. *Colloid Polym. Sci.* **1975**, *253*, 566–580. [CrossRef]

54. Deng, W.; Jeng, D.S.; Toorop, P.E.; Squire, G.R.; Iannetta, P.P.M. A mathematical model of mucilage expansion in myxospermous seeds of Capsella bursa-pastoris (*Shepherd's purse*). *Ann. Bot.* **2012**, *109*, 419–427. [CrossRef] [PubMed]

55. Davarcı, F.; Turan, D.; Ozcelik, B.; Poncelet, D. The influence of solution viscosities and surface tension on calcium-alginate microbead formation using dripping technique. *Food Hydrocoll.* **2017**, *62*, 119–127. [CrossRef]

56. Rentería-Ortega, M.; Salgado-Cruz, M.D.L.P.; Morales-Sánchez, E.; Alamilla-Beltrán, L.; Farrera-Rebollo, R.R.; Valdespin-León, M.; Calderón-Domínguez, G. Effect of electrohydrodynamic atomization conditions on morphometric characteristics and mechanical resistance of chia mucilage-alginate particles. *CYTA J. Food* **2020**, *18*, 461–471. [CrossRef]

57. Santhanes, D.; Teng, L.Y.; Sheng, F.S.; Coombes, A.G.A. Exploiting the versatility of oral capsule formulations based on high M-alginate for targeted delivery of poorly water soluble drugs to the upper and lower GI tract. *J. Drug Deliv. Sci. Technol.* **2018**, *46*, 384–391. [CrossRef]

58. Estrada-Villegas, G.M.; Martínez-Hernández, R.C.; Morales, J.; Olayo, R. Incorporation of fluoroquinolone/beta cyclodextrin inclusion complex from polylactic acid electrospun fibers and modeling of the release behavior. *Rev. Mex. Ing. Quim.* **2019**, *18*, 737–747. [CrossRef]

59. Nayak, A.K.; Pal, D.; Pradhan, J.; Hasnain, M.S. Fenugreek seed mucilage-alginate mucoadhesive beads of metformin HCl: Design, optimization and evaluation. *Int. J. Biol. Macromol.* **2013**, *54*, 144–154. [CrossRef]

60. Velázquez-Gutiérrez, S.K.; Figueira, A.C.; Rodríguez-Huezo, M.E.; Román-Guerrero, A.; Carrillo-Navas, H.; Pérez-Alonso, C. Sorption isotherms, thermodynamic properties and glass transition temperature of mucilage extracted from chia seeds (*Salvia hispanica* L.). *Carbohydr. Polym.* **2015**, *121*, 411–419. [CrossRef]

61. Javanbakht, V.; Shafiei, R. Preparation and performance of alginate/basil seed mucilage biocomposite for removal of eriochrome black T dye from aqueous solution. *Int. J. Biol. Macromol.* **2020**, *152*, 990–1001. [CrossRef] [PubMed]

62. Ritger, P.L.; Peppas, N.A. A simple equation for description of solute release II. Fickian and anomalous release from swellable devices. *J. Control. Release* **1987**, *5*, 37–42. [CrossRef]

63. Xin, F.; Sui, M.; Liu, X.; Zhao, C.; Yu, Y. Biodegradable poly(N-isopropylacrylamide-co-N-maleylgelatin) hydrogels with adjustable swelling behavior. *Colloid Polym. Sci.* **2019**, *297*, 763–769. [CrossRef]

64. Bajpai, A.K.; Bajpai, J.; Shukla, S. Water sorption through a semi-interpenetrating polymer network (IPN) with hydrophilic and hydrophobic chains. *React. Funct. Polym.* **2002**, *50*, 9–21. [CrossRef]

65. Montoya-Álvarez, M.; Quinchía-Figueroa, A.M.; González-Murillo, O.; Araque-Marín, P. An evaluation of the controlled release of ammoniacal nitrogen from residual cellulose/polyvinyl alcohol hydrogels as an alternative to traditional fertilization processes. *Dyna* **2018**, *85*, 187–193. [CrossRef]

66. Zhang, H.; Zhang, Y.; He, L.; Yang, B.; Zhu, S.; Yao, M. Thermal-responsive poly (*N*-isopropyl acrylamide)/sodium alginate hydrogels: Preparation, swelling behaviors, and mechanical properties. *Colloid Polym. Sci.* **2016**, *294*, 1959–1967. [CrossRef]

67. Peppas, N.A.; Franson, N.M. The swelling interface number as a criterion for prediction of diffusional solute release mechanisms in swellable polymers. *J. Polym. Sci. Polym. Phys. Ed.* **1983**, *21*, 983–997. [CrossRef]

68. Ruiz-Ruiz-Riancho, N.; Garcia, A.; Grossegger, D.; Saadoon, T.; Hudson-Griffiths, R. Properties of ca-alginate capsules to maximise asphalt self-healing properties. *Constr. Build. Mater.* **2021**, *284*, 122728. [CrossRef]